Journal of Casting & Materials Engineering Vol. 6 No. 1 (2022) 14–21
https://doi.org/10.7494/jcme.2022.6.1.14

Structural and Morphological Evaluations of Natural Hydroxyapatite from Calcined Animal Bones for Biomedical Applications

Olusola Emmanuel Ojo[a,b*], Olatunde Israel Sekunowo[a], Margaret Okonawan Ilomuanya[c], Oluwashina Philips Gbenebor[a], Samson Oluropo Adeosun[a]

[a]University of Lagos, Faculty of Engineering, Department of Metallurgical & Materials Engineering, Akoka, Lagos, Nigeria
[b]Federal Institute of Industrial Research, Projects Development and Design Department, Cappa Bus Stop, Oshodi, Lagos, Nigeria
[c]University of Lagos, Faculty of Pharmacy, Department of Pharmaceutics and Pharmaceutical Technology, Idi– Araba, Lagos, Nigeria
e-mail: isolyet@yahoo.com

Received: 28 October 2021/Accepted: 17 January 2022 Published online: 8 February 2022
This article is published with open access at AGH University of Science and Technology Press.

Abstract

Several biomedical materials have been employed as drug delivery systems, but natural Hydroxyapatite (HAP) has been proven to be exceptionally better than other materials owing to its excellent bioactivity and biocompatibility properties. In this study, natural HAP was obtained from bovine and caprine bones and comparatively analysed for biomedical applications. The bones were hydrothermally treated, calcined in the temperature range of 700–1100°C, held for 2 hours in an electric furnace to remove the organic contents; milled, sifted with 150 µm mesh sieve and then characterized. It was revealed by Energy Dispersive X-Ray Spectroscopy (EDS) that the bovine and caprine bone samples calcined at 1000°C had calcium/phosphorus ratio (Ca/P) of 1.66 closest to the standard of 1.67. The bovine HAP showed the best crystallinity (86.23%) at 1000°C while caprine HAP had its highest (87.25%) at 1100°C. Fourier Transform Infrared Spectroscopy (FTIR) results revealed that the calcination temperature must be greater than 700°C to isolate high quality HAP. The Scanning Electron Microscopy (SEM) showed that the samples calcined at 800°C had the largest average particle size (85.34 µm) while porosity increases with calcination temperature in both samples. The HAP obtained at a calcination temperature of 1000°C proved to have the best quality for biomedical applications.

Keywords:

hydroxyapatite, calcination, animal bones, crystallinity, porosity

1. INTRODUCTION

The animal bone comprises 65–70% inorganic components and 30–35% organic at the molecular level [1]. Collagen (95%) is the main component of the organic part of the bone with proteins [2]. There are other organic substances like chondroitin sulphate and keratin sulphate with different lipids like phospholipids, fatty acids and cholesterol [3] in minute quantities. The inorganic part of the bone is mainly hydroxyapatite (HAP) $Ca_{10}(PO_4)_6(OH)_2$, which belongs to the group of calcium/phosphate-based biomaterial of ceramic origin with considerable chemical similarity to the inorganic constituent of the bone matrix [4]. Generally, apatite is described by means of the chemical formula $M_{10}(XO_4)_6Z_2$ where M could be Ca^{2+}, Mg^{2+}, Na^{+}, Zn^{2+}, Sr^{2+}, Ba^{2}+, Pb^{2+}or Si^{2+}; X could be P^{5+}, Cr^{5+}, V^{5+} or Mn^{5+} and Z could be Cl^{-}, F^{-} or OH^{-} [5]. HAP is a non-toxic, biocompatible, non-inflammatory and non-immunogenic agent. It is also bioactive because it has the ability to form a bond with the surrounding bone tissue after implantation. Many studies have been carried out on it owing to its chemical and structural similarity to bone minerals [6, 7]. As a result of these properties, it is considered to play a vital role in both medical and nonmedical fields such as drug delivery, orthopedics, dentistry, maxillofacial, skull defects, wound tissue engineering, artificial bone synthesis, biosensor, the removal of heavy metals, and the removal of nitrate from water [8, 9]. HAP can be derived from either a natural source like marine sources (fish bone and fish scale), shell sources (seashell and eggshell) and mineral sources (limestone) [10] or by synthetic methods like sol-gel, wet chemical precipitation, hydrothermal method, microwave irradiation [11–14] etc. Comparatively, natural apatite existing in bones has better biological properties than synthesized HAP. In this regard, researchers have endeavored to isolate HAP scaffolds from natural sources [15] because of the presence of beneficial cations such as Na^{+}, K^{+}, Zn^{2+}, Si^{4+}, Mg^{2+}, Ba^{2+} and anions such

as F^-, CO_3^{2-} etc., which are considered to play important roles in tissue engineering and other biochemical reactions [16]. The trace elements are actively involved in the natural bone metabolism process, while the carbonate ions considered as an impurity in natural HAP help to enhance the mechanical strength, bioactivity and bio-resorbability of the implants. This makes natural HAP highly beneficial and more suitable in some applications (like drug delivery) than synthetic HAP [17, 18]. In this study, caprine and bovine bones were calcined to isolate their HAP and then comparatively analyzed for compositions and physico-chemical properties in relation to biomedical applications. Ojo *et al*. [19] have claimed that, despite their availability, the use of caprine bones has been understudied.

2. MATERIALS AND METHODS

2.1. Preparation of bovine and caprine bone particles

The femur bones of bovine (*Bos Taurus*) and caprine (*Capra aegagrus hircus*) used in this research work were acquired from the Magboro main market in Ogun State, Nigeria. The bovine bones were obtained from ~36 months old and caprine bones from 30–36 months old animals. The dirt and blood on the bone surfaces were washed off thoroughly and then soaked for 96 hours in water to break the firmly adhering tissues, meat, and other impurities on the surface. The bones were broken into 4–10 cm lengths and the marrow were removed. Defatting of the bones was done to remove the proteins and fatty substances in a 10-litre Quink® pressure pot with 4 L of preheated water poured and heated to 120°C for 1.5 hours. On cooling, the bones were then oven dried for 8 hours at 80°C. After drying, calcination was done to remove the organic matter (collagen) present in the bone samples. The bovine and caprine bones were placed into a laboratory furnace (Carbonite, England) with 16,000 cm^3 heating chamber at 10°C/min heating rate for calcination at 700, 800, 900, 1000 and 1100°C; soaked for 2 hours and left overnight to cool to ambient temperature in the furnace. Each of the calcinations was started at the minimum temperature possible in the heating chamber at the beginning of each day. The calcined bone samples were subjected to hammer milling using Broyeur Clero® (Model 13634, 1.5 kV, France). This process facilitated bone size reduction to less than 10mm. Then the bone particles were ball milled using a Faure®machine (Model 28A20:92, France) with 5 kg-ceramic milling balls of 10–20 mm diameter in a 10-litre milling barrel. Ball milling was done at the speed of 40 rpm for 20 hours and then sifted with 150 μm mesh sieve before characterization.

2.2. Physicochemical and morphological characterization

EMPYERN XRD-600 Diffractometer (45 kV, 40 mA) with a CuKα (λ = 1.54 Å) was used to determine the phase composition of the samples. Radiation over the scanning range (2θ) from 5° to 75° and a step size of 0.026°. Using the Equation (1) used by Rana et al. [15], the degree of crystallinity was obtained.

$$X_c(\%) = 1 - \frac{V_{112/300}}{I_{300}} \tag{1}$$

where:

$V_{112/300}$ – intensity of the valley (hollow part) between peaks 112 and 300;
I_{300} – intensity of peak 300.

Similarly, the crystallite size (*D*) was determined using Scherrer's equation:

$$D = \frac{K\lambda}{\beta\cos\theta} \tag{2}$$

where:

K – constant for spherical crystallite; K = 0.89;
β – full width at half maximum of the peak in radians;
λ – diffraction wavelength (0.154059 nm);
θ – diffraction angle.

The functional groups present in the bovine bone samples (BBS) and caprine bone samples (CBS) were confirmed using Agilent Technologies® (USA) FTIR analyzer in the range of 4000–650 cm^{-1}. The morphology of the BBS and CBS were examined using SEM; model Phenom® Eindhoven, Netherlands. The EDS that was equipped with the SEM was used to analyze the elemental composition of the samples. The chemical composition of the BBS and CBS bone samples were revealed by XRF analyzer while the porosity was determined by analyzing the SEM micrographs 5 times each using Image J® software and the average values were recorded.

3. RESULTS AND DISCUSSION

3.1. General observations

During the calcination process of the bone samples, between 170°C and slightly greater than 700°C, pungent and choking fumes were observed from the furnace exhaust pipe. This is the temperature range at which the organic component decomposed. The pH of the fumes was ~9 when tested with damp litmus paper. Brownish and bluish colour patches were observed on the bone samples, especially the bovine ones calcined at 1100°C. It was also observed that at 800°C, the physicochemical properties of both bone samples were all deviant unlike the properties at other calcination temperature. The calcination was repeated at the temperature (800°C) for confirmation; the same results were obtained. This might indicate that 800°C is a transitional temperature in the calcination process.

3.2. Bone calcination

The HAP was extracted from the bovine and caprine bones by means of the thermal decomposition process. In the process, at highest calcination temperature (1100°C), the largest quantity of organic matter (collagen) was dispelled.

After calcination at this temperature, there was a 40.6% and 45.6% weight reduction, which signifies the quantity of collagen dispelled in BBS and CBS respectively. This was as a result of the enormous heat generated at this temperature (1100°C), which was high enough to rid the bone samples of the inorganic content, in contrast to what happened at 700°C where only 31.2% of the collagen was eliminated from the BBS. The black color of the sample calcined at 700°C revealed the incomplete removal of the organic matrix within the bone. Consequently, calcination at temperature close to 700°C is not beneficial for removing residual organic content for the isolation of pure HAP from the bone samples. As expected, the percentage weight loss is directly proportional to the calcination temperature (Fig. 1).

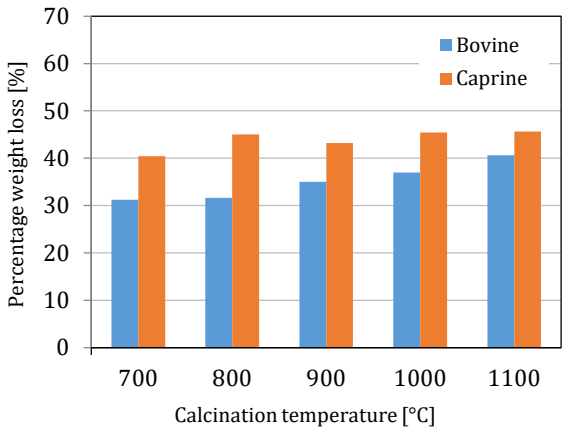

Fig. 1. Percentage weight loss in calcined BBS and CBS at different calcination temperature

3.3. Chemical composition of calcined bone

The XRF analysis results of the calcined and raw BBS and CBS at different calcination temperature are presented in Tables 1 and 2 showing the chemical compositions of these materials in oxide form. Oxides of calcium and phosphorous are the main components in the bone samples with phosphoric pentoxide (P_2O_5) and calcium oxide (CaO) as 31.08 wt.% and 40.36 wt.% in BBS; 30.90 wt.% and 41.96 wt.% in CBS respectively. The loss on ignition (LOI) of raw BBS and CBS were 26.64% and 24.89% respectively. The LOI indicates the removal of the inorganic substance of the bone samples, which is probably the reason for its absence in the calcined samples. The iron III oxide (Fe_2O_3) and copper II oxide (CuO) which are known for their brownish and bluish color respectively could have been concluded to be responsible for the coloration of the samples at calcination temperature of 1100°C, but their quantity in the raw samples were negligible. Magnesium oxide, strontium oxide, silica, and copper oxide were found in very minute quantities in both bone samples.

3.4. Elemental composition of calcined bones

The elemental composition of the raw and calcined BBS and CBS at different calcination temperature were investigated by EDS analysis as shown in Tables 3 and 4.

Table 1
Oxide composition of raw and calcined BBS at different calcination temperature in weight percentage

Oxides	Raw	700°C	800°C	900°C	1000°C	1100°C
CaO	40.36	52.36	25.38	46.79	46.40	46.92
P_2O_5	31.80	40.95	22.07	38.83	45.33	48.91
Fe_2O_3	0.19	0.019	0.52	0.024	0.05	0.02
SiO_2	0.18	0.33	7.70	0.67	1.52	0.68
MgO	0.43	1.65	0.88	0.66	1.22	–
CuO	0.016	–	0.0011	–	0.004	0.0002
SrO	0.15	1.26	0.59	0.81	1.02	0.86
Others	0.234	3.431	42.86	12.22	4.456	2.61
LOI	26.64	–	–	–	–	–

Table 2
Oxide composition of raw and calcined CBS at different calcination temperature in weight percentage

Oxides	Raw	700°C	800°C	900°C	1000°C	1100°C
CaO	41.95	52.61	45.14	50.47	46.44	47.44
P_2O_5	30.90	40.36	38.00	40.94	45.00	51.16
Fe_2O_3	–	0.04	0.22	0.19	0.03	0.13
SiO_2	0.20	0.51	3.81	0.56	1.32	0.89
MgO	0.50	0.64	1.27	0.46	1.16	–
CuO	0.006	–	–	–	0.0003	0.000064
SrO	0.20	2.07	1.24	2.17	1.17	1.13
Others	1.354	3.77	10.32	5.21	4.88	–
LOI	24.89	–	–	–	–	–

Table 3
Elemental composition of calcined BBS at different calcination temperature in weight percentage

Elements	Raw	700°C	800°C	900°C	1000°C	1100°C
Ca	50.44	69.43	55.69	66.24	66.19	63.97
P	16.75	18.33	20.68	18.26	23.08	23.27
Mg	0.66	0.53	2.38	0.70	0.91	1.08
K	0.6	0.62	0.97	1.00	0.53	0.67
Na	0.5	0.58	1.12	0.43	0.75	0.87
C	17.17	1.07	0.89	1.34	1.10	1.36
O	5.99	–	–	–	–	–
Ag	1.86	1.20	1.30	1.89	1.54	1.63
Si	1.55	0.48	4.93	0.65	0.52	0.6
N	1.46	–	0.19	–	0.39	0.28
Al	1.33	0.40	4.16	0.63	0.63	0.73
S	0.72	0.16	0.5	0.36	0.34	0.30

Table 4
Elemental composition of calcined CBS at different calcination temperature in weight percentage

Elements	Raw	700°C	800°C	900°C	1000°C	1100°C
Ca	44.31	66.91	62.96	66.93	65.29	64.73
P	13.8	18.58	21.73	18.48	22.77	23.0
Mg	0.52	0.59	1.96	0.80	0.97	1.12
K	0.33	0.81	0.75	0.99	0.56	0.57
Na	0.26	0.39	0.72	0.56	0.52	0.62
C	30.02	1.18	0.81	1.03	2.30	0.93
O	5.17	–	–	–	–	–
Ag	0.94	1.92	1.82	1.66	1.42	1.56
Si	2.2	0.65	1.38	0.72	0.72	0.49
N	–	–	0.16	–	0.60	0.38
Al	1.70	0.94	1.51	0.81	0.69	0.61
S	0.75	0.38	0.33	0.55	0.31	0.32

Calcium, carbon, phosphorus and oxygen were present in significant amounts in both raw and calcined bone samples while the presence of trace beneficial elements such as sodium, magnesium, potassium and silicon were detected also in the crystal lattice of the isolated HAP. Carbon and oxygen were significantly present in both raw samples, with traces of sulfur, and nitrogen as they were the main constituents of collagen being a protein. Carbon in raw samples reduced from 17.7% to 1.36% and 30.02% to 0.93% at 1100°C in BBS and CBS respectively. Similarly, as the calcination temperature increases, oxygen is driven off from the organic substance [20]. The composition of these elements reduced drastically as the calcination was carried out on both samples. This might not be unconnected with the fact that the calcination process expelled the organic substance; consequently, the elements that make up the organic substance will be reduced in the crystal lattice of the samples after calcination. The sum of the weight percentage of the carbon and oxygen present in raw CBS is more than that of BBS. This is also in accordance with the results in Figure 1, where the percentage weight loss of calcined CBS is more than that of BBS at any calcination temperature, indicating that CBS has a higher percentage of organic substances. The percentage of phosphorus in the raw samples was found to have increased from 16.75% to 23.27% and 13.8% to 23.0% at 1100°C in BBS and CBS respectively while calcium in the raw samples was found to increase from 50.44% to 63.97% and 44.31% to 64.73% at 1100°C in BBS and CBS respectively. This implies that calcium and phosphorus increase together with an increase in calcination temperature because of the other elements (Carbon and oxygen) that were eliminated as the calcination temperature increases. Similar to the work of Venkatesan & Kim [21], the increase does not tend to be directly proportional to the temperature increase.

The Ca/P ratios of calcined BBS and CBS are presented in Figure 2. The Ca/P ratio for the two calcined bone samples from 700 to 1100°C show deviations from the theoretical value for pure stoichiometric HAP of 1.67. In fact, natural HAP is non-stoichiometric (exhibits a Ca/P ratio higher than 1.67) [22]. The Ca/P ratios of HAP derived from both bone samples obtained at 1000°C have the closest values of 1.66.

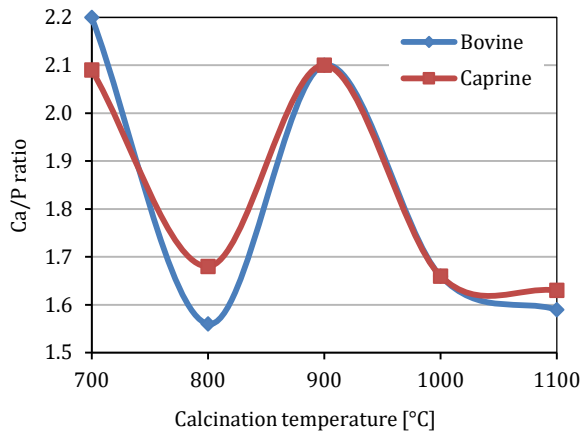

Fig. 2. Calcium-to-Phosphorus ratio of BBS and CBS at different calcination temperature

The range of Ca/P ratio of HAP derived from both samples in the present study appear to be markedly higher at 1.59–2.20 compared to those reported from recent study by Ramesh et al. [18] at 1.58–1.88. Also, the CBS is higher at 1.63–2.09 compared with 1.61–1.79. Researchers have been able to identify the factors that could contribute to the deviation of Ca/P ratio from the theoretical value of 1.67. These are calcination conditions like the holding temperature and atmosphere of the calcination process. These will significantly affect the quantity and type of calcium compounds which would appear in the resultant HAP phase [23]. Moreover, ions such as Ca^{2+}, PO_4^{3-} and OH^- exist in natural tissues and their intensity may vary depending on the nutrition and diet of the animal [24].

3.5. Identification of functional groups in HAP

The FTIR has been extensively used for identification of the characteristic functional groups in HAP. These include phosphate (PO_4^{3-}), hydroxyl (OH^-) and carbonate (CO_3^{2-}). In this study, BBS and CBS, the (CO_3^{2-}) appeared at 872 cm^{-1}, 1409–1424 cm^{-1} and 1446–1484 cm^{-1}, the presence of (OH^-) was shown at 3571 cm^{-1}. The (PO_4^{3-}) was revealed at the 913 cm^{-1}, 1006–1029 cm^{-1}, 1088 cm^{-1} and 2013–2020 cm^{-1}. The FTIR spectra of raw and calcined BBS and CBS at 700–1100°C are shown in Figures 3 and 4.

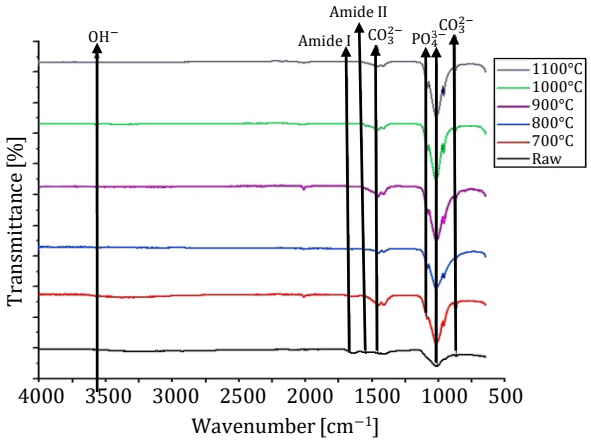

Fig. 3. FTIR spectra of raw and calcined BBS at different calcination temperature

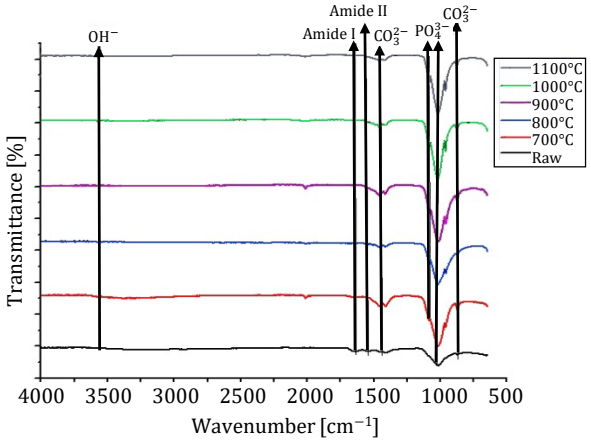

Fig. 4. FTIR spectra of raw and calcined CBS at different calcination temperature

The raw BBS showed characteristic band of amide I and II at 1640 cm^{-1} and 1543 cm^{-1} also for CBS at 1636 cm^{-1} and 1543 cm^{-1} respectively. This is due to the presence of the organic moieties in the raw samples. The HAP obtained from BBS and CBS at 700°C showed all the characteristic bands of the HAP with amide I band, which means the presence of collagen but from calcination temperature of 800–1100°C, all the collagen bands start to disappear. The intensities of both amide bands I and II are lower in the BBS than CBS, which implies that the former has a lower amount of organic phase than the latter. As the calcination temperature increases, the amide I peak gradually reduces until it totally disappeared at 800°C in BBS and 900°C in CBS. Amide II disappeared completely at 700°C in both samples. Moreover, the appearance of an additional peak at 962–958 cm^{-1} and 1088 cm^{-1} due to the symmetrical stretching of phosphate (PO_4^{3-}) in the bones calcined at temperature above 700°C, which was not present in raw BBS and CBS, indicates that the shielded HAP was being freed from organic matter at high temperature. The most intensive and sharpest bands in the range of 1021–1034 cm^{-1} correspond to asymmetric stretching vibrations ($\nu 3$). Its intensity increases with the increase in calcination temperature. Further, the bands between 2080–2013 cm^{-1} due to the overtones and combination of the $\nu 3$ and $\nu 1$ (PO_4^{3-}) were also observed but the intensity of the $\nu 2$ was found to decrease with the increase in the temperature of calcinations. With the increase of the calcination temperature, the relative intensities of the OH^- vibration bands, which did not appear in both raw samples but started appearing at 800–1100°C at band 3571 cm^{-1} for CBS and only from 900–1100°C BBS, show a decrease in intensity in the CBS and thus indicating the process of dehydroxylation, where OH^- is released by the formation of water molecules. The HAP isolated from BBS showed bands between 1461–1446 cm^{-1} and 1420–1409 cm^{-1} and CBS at 1484–1446 cm^{-1} and 1424–1409 cm^{-1} at calcination temperature range of 700–1100°C due to asymmetric stretching or $\nu 3$ of carbonate. The weak band in BBS and CBS at 872–880 cm^{-1} shows out of plane carbonate band, which disappear as the temperature increases [25] and a small band at 667 cm^{-1} for raw CBS, which is associated with the bending vibration of a hydroxyl group of HAP [26]. There was no visible OH^- in both samples at 3571 cm^{-1} before heating but after, which is possibly because of overlapping of impurity bands or masking effect of other impurity bands over it [15]. The absorbed water band (3276 cm^{-1}) appeared in the raw sample and the one calcined at 700°C in BBS and CBS but disappeared with the increase in calcination temperature. It must be noted that the intensities and position of the corresponding absorption bands may be caused by the change in the molecular environment of the HAP [27].

3.6. Crystallographic analysis of calcined HAP

The phase composition analysis of the samples was performed. Figures 5 and 6 show the XRD patterns of raw and calcined BBS and CBS obtained by varying the calcination temperature from 700–1100°C. The XRD parameters of BBS and CBS show identical phases present. The intensities of BBS and CBS dispersed by X-ray radiation were found to be 609 and 573 au respectively, which are relatively low intensities with a wider peak. This is due to the strong presence of organic contents (collagen) in the bone. The amorphous phase disappeared as the calcination temperature increases. It was observed that as the calcination temperature increases, the peak intensity increases with a decrease in the width of the peak, indicating the removal of the organic portion. This also means increasing crystalline nature and crystal size. The CBS in all the calcination temperature was revealed to have lower HAP peak intensities than the BBS. This might not be unconnected with the presence of higher organic content in CBS than that of BBS as revealed during the calcination process. The samples calcined at 700°C in both samples showed wider peak of low intensity, which was a slight improvement over the raw samples, indicating the incomplete removal of organic matter present in the bone matrix. However, thermal calcinations from 800°C showed intense and sharp peaks indicating the crystalline nature and complete removal of organic matter. Blanco et al. [28] revealed that the highest diffraction peak height is related to the amount of crystalline material in the sample. This showed that both raw and calcined CBS have lower crystalline HAP phase when compared with BBS, which indicates more amorphous collagen than the BBS. The XRD patterns of the samples at the range of calcination temperature used in this study do not reveal any other peak apart from HAP's. This is an indication that the HAP derived from the two samples showed thermal stability even at the highest temperature (1100°C) [18].

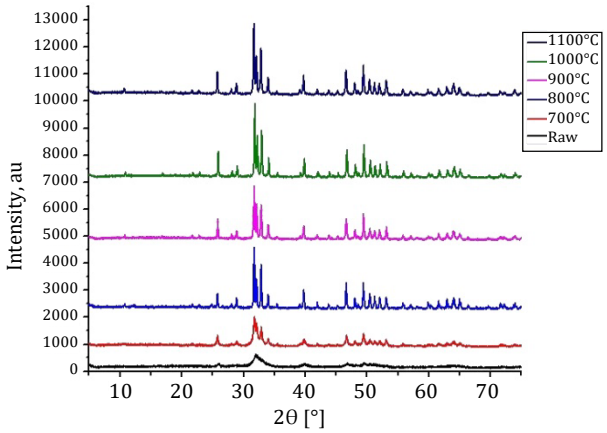

Fig. 5. XRD pattern of raw and calcined BBS at different calcination temperature

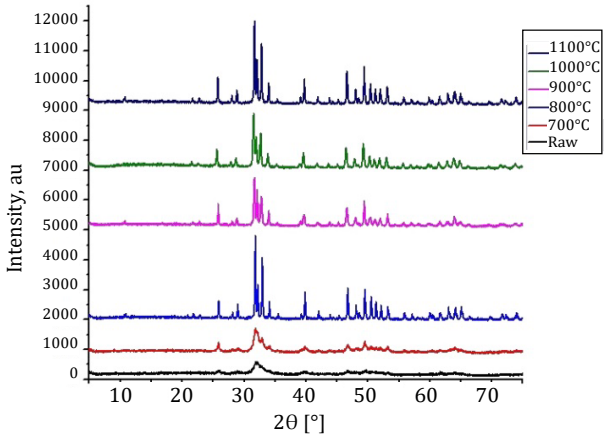

Fig. 6. XRD pattern of raw and calcined CBS at different calcination temperature

Table 5 shows the parameters obtained from XRD spectra; the peak intensity, crystallinity index and crystallite size obtained at the different calcination temperatures. There is no separated peak between 112 and 300. It is important to note that dehydroxylation of the HAP phase would cause a small degree of peak shifting in the XRD trace.

Table 5
Crystallographic parameters of raw and calcined BBS and CBS at different calcination temperature

Temperature	Samples	Intensity peak [au]	Crystallinity index [%]	Crystallite size [nm]
Raw	Bovine	609	No separated peaks	–
	Caprine	573	No separated peaks	–
700°C	Bovine	1201	50.8	39.88
	Caprine	910	24.79	39.89
800°C	Bovine	2410	83.47	53.18
	Caprine	2937	88.17	53.19
900°C	Bovine	2073	84.5	53.18
	Caprine	1729	78.77	45.57
1000°C	Bovine	2871	86.23	53.79
	Caprine	1956	75.31	40.31
1100°C	Bovine	2749	83.4	53.78
	Caprine	2890	87.25	53.78

The degrees of crystalline and crystallite size in both samples tend to increase with an increase in calcination temperature. Zhang et al. [29] revealed that increasing crystallinity of nCaP could slow drug release rate. Also, lower crystallinity exhibited higher drug loading capacity due to presence of more Ca^{2+} adsorption sites on the surface. Similarly, Sanosh et al. [30] reported that the HAP with high crystallinity have little or no activity towards bio-resorption, which is important for the formation of chemical bonding with surrounding hard tissues and fully developed crystalline HAP structure is insoluble in physiological environment expected to be less metabolically active than the crystalline HAP. Additionally, the crystallite size was not consistent with calcination temperature; it was believed that crystal size was closely related to the age of the animal, especially the age of the crystal. The crystal harvested from young postnatal animals was reported to be shorter and thicker than that from mature individual [31].

When crystallinity index (X_c) ≥ 70% usually considered to be a high degree of crystal; 30% < X_c < 70% Medium degree of crystal and when X_c < 30%, it is considered low degree of crystal.

3.7. Calcined HAP morphology and size examination

The scanning electron micrographs and average particle size of the raw and calcined BBS and CBS at 700–1100°C are presented in Table 6 and Figure 7.

Table 6
Average particle size of raw and calcined BBS and CBS at different temperature in micrometer

Samples	Raw	700°C	800°C	900°C	1000°C	1100°C
BBS	52.4	15.52	85.34	12.36	8.35	8.14
CBS	40.7	13.13	88.31	10.01	7.14	7.04

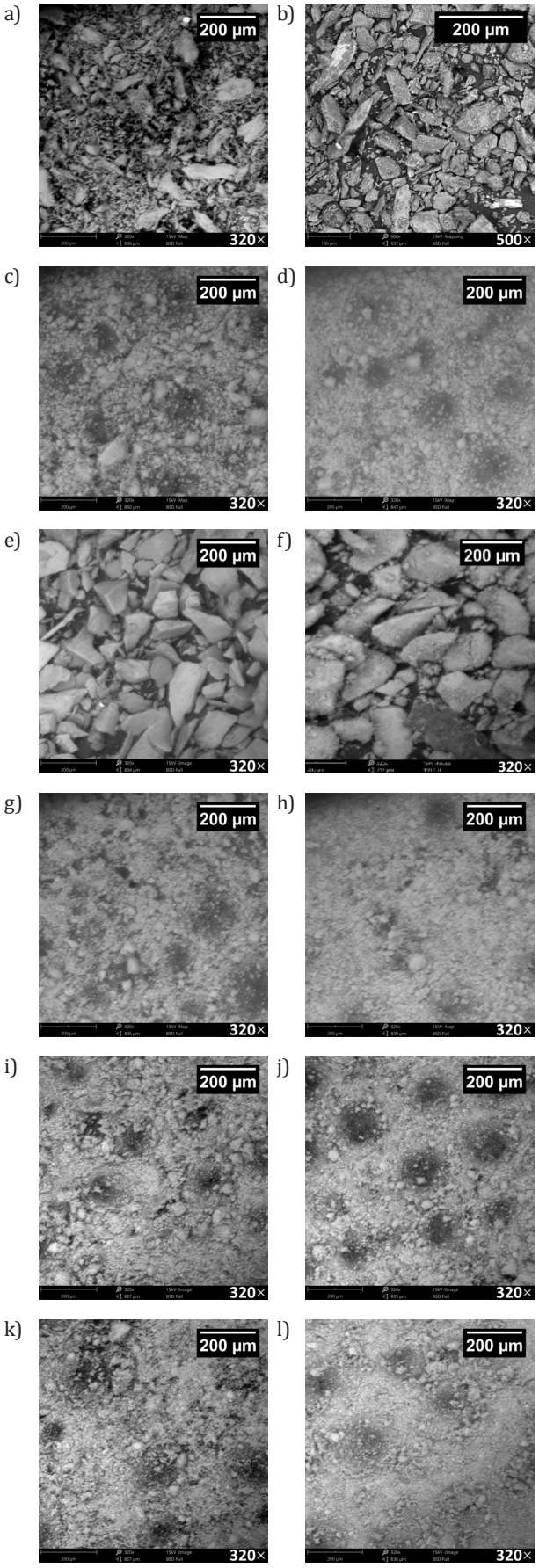

Fig. 7. SEM Morphology of raw and calcined BBS and CBS: a) BBS Raw; b) CBS Raw; c) BBS 700°C; d) CBS 700°C; e) BBS 800°C; f) CBS 800°C; g) BBS 900°C; h) CBS 900°C; i) BBS 1000°C; j) CBS 1000°C; k) BBS 1100°C; l) CBS 1100°C

The morphologies of raw BBS and CBS look like mass of aggregates that have low surface area and show a wide range of particle size and shapes with edges and corners rather than being spherical. This irregularity in size and shape of the particles might be due to the presence of collagen in the raw samples, which means more toughness and subsequently more resistance to milling [19]. In comparison, the calcined bone samples show some alteration in their mophologies and particle size reduction was maximal, exhibiting higher surface area [32]. This might be attributed to less energy requirement for their size reduction as the organic moiety, which served as the matrix had been eliminated by heat generated at high temperature of the calcination process. Calcined samples at 700°C tend to have a larger particles size, more noticeable in BBS. This might be due to the incomplete removal of collagen. The particles become finer as the calcination temperature increases. The particle size, shape and surface roughness have effect on the properties of the particles. The particle size plays an important role in the drug release profile of the particles [33]. Moreover, the morphology of HAP particles also depends on the source of the bone, holding time and temperature of calcination. It might also be influenced by the gender, age, and food habit of the animals from which the bone was collected. Hence, more studies are required to understand the influence of these biological factors on the morphology.

3.8. Porosity analysis of calcined HAP

The porosity of the calcined BBS and CBS at different temperature is shown in Table 7. Porous HAP is an excellent drug carrier. Netz et al. [34] conducted in vitro tests to show that the porosity of HAP greatly influenced drug release kinetics by using HAP with high porosity (82.63%), which exhibited irregular release of cisplatin as high porosity could cause an irregular structure, which may have affected the cisplatin release. The HAP porosity would be useful in the drug delivery systems, only if the porosity is less than 78%. HAP of lower porosity showed significant initial burst release. It was believed that a higher porosity could provide more motion freedom of the molecules to be regularly carried out from the porous structure of HAP. The porosity in the two samples reduces with increase in calcination temperature. This may be attributed to the tighter packing of HAP at a high temperature, due to the improved crystallinity of the structure [35]. Also, the loading efficiency increases with porosity [17].

Table 7
Porosity of raw and calcined BBS and CBS at different temperature in percentage

Samples	Raw	700°C	800°C	900°C	1000°C	1100°C
BBS	43.1	38.7	29.37	34.84	33.56	32.92
CBS	25.6	40.42	24.71	36.32	31.20	28.64

4. CONCLUSIONS

In this research, the best Ca/P ratio of 1.66, which is close to the standard (1.67) was obtained at 1000°C. On average, the BBS HAP had the highest degree of crystallinity (86.23%) at 1000°C while CBS HAP had its (87.25%) at 1100°C. It was also observed that calcination at 700°C gave HAP of the worst quality. The composition, morphology and particle size of samples calcined at 800°C were deviant unlike the properties at other calcination temperature. It might be a transition temperature at which the cohesive forces are broken down in the samples. The calcination affected the quantity of major elements like calcium and phosphorus that increase with temperature. In contrast, other elements like carbon, oxygen, sulfur that are associated with organic moieties reduced drastically at the elevated temperature. The minor elements like sodium, magnesium etc., were still present in the HAP even at the highest temperature (1100°C). The calcined bone samples when compared with raw samples showed some alteration in its morphology with spherical agglomerates in high surface area HAP particles. There was particle size and porosity reduction with increase in calcination temperature in both samples. At 1100°C and 800°C, the smallest and largest particle size respectively were recorded with BBS and CBS having 8.14 μm and 7.04 μm also 85.34 μm and 88.31 μm particle size respectively. Samples calcined at 1100°C had the least porosity. However, a calcination temperature of 1000°C has proven to be the best temperature for the isolation of the best quality HAP from both BBS and CBS.

REFERENCES

[1] Khandelwal H. & Prakash S. (2016). Synthesis and characterization of hydroxyapatite powder by eggshell. *Journal of Minerals and Materials Characterization and Engineering*, 4(2), 119–126. Doi: https://dx.doi.org/10.4236/jmmce.2016.42011.

[2] Venkatesan J., Lowe B., Manivasagan P., Kang K.-H., Chalisserry E.P., Anil S., Kim D.G. & Kim S.-K. (2015). Isolation and characterization of nano-hydroxyapatite from salmon fish bone. *Materials*, 8(8), 5426–5439. Doi: https://doi.org/10.3390/ma8085253.

[3] Bano N., Jikan S.S., Basri H., Adzila S. & Zago D.M. (2019). XRD and FTIR study of A&B type carbonated hydroxyapatite extracted from bovine bone. In: *Proceedings of the AIP Conference*, AIP Publishing, Article ID 020100.

[4] Zhu Y., Murali S., Stoller M.D., Ganesh K.J., Cai W., Ferreira P.J., Pirkle A., Wallace R.M., Cychosz K.A. , Thommes M., Su D., Stach E.A. & Ruoff R.S. (2011). Carbon-based supercapacitors produced by activation of graphene. *Science*, 332(6037), 1537–1541. Doi: https://doi.org/10.1126/science.1200770.

[5] Shalaby S.W. & Salz U. (Eds.) (2007). Polymers for dental and orthopedics applications. *Boca Raton*: CRC Press.

[6] Fahmy M.D., Jazayeri H.E., Razavi M., Masri R. & Tayebi L. (2016). 3-Dimensional bioprinting materials with potential application in preprosthetic surgery. *Journal of Prosthodontics*, 25(4), 310–318. Doi: https://doi.org/10.1111/jopr.12431.

[7] Dhandayuthapani B., Yoshida Y., Maekawa T. & Sakthi Kumar D. (2011). Polymeric scaffolds in tissue engineering application: A review. *International Joutnal of Polymer Science*, Article ID 290602. Doi: https://doi.org/10.1155/2011/290602.

[8] Manalu J.L. Soegijono B. & Indrani D.J. (2015). Characterization of hydroxyapatite derived from bovine bone. *Asian Journal of Applied Sciences*, 3(4), 758–765.

[9] Rajesh R., Hariharasubramanian A. & Ravichandran D. (2012). Chicken bone as a bioresource for the bioceramic (hydroxyapatite). *Phosphorus, Sulfur, and Silicon and the Related Elements*, 187(8), 914–925. Doi: https://doi.org/10.1080/10426507.2011.650806.

[10] Mohd Pu'ad N.A.S., Koshy P., Abdullah H.Z., Idris M.I. & Lee T.C. (2019). Syntheses of hydroxyapatite from natural sources. *Heliyon*, 5(5), e01588. Doi: https://doi.org/10.1016/j.heliyon.2019.e01588.

[11] Agrawal K., Singh G., Puri D. & Prakash S. (2011). Synthesis and characterization of hydroxyapatite powder by Sol-Gel method for biomedical application. *Journal of Minerals and Materials Characterization and Engineering*, 10(8), 727–734. Doi: https://doi.org/10.4236/jmmce.2011.108057.

[12] Gentile P., Wilcock C.J., Miller C.A., Moorehead R. & Hatton P.V. (2015). Process optimisation to control the physico-chemical characteristics of biomimetic nanoscale hydroxyapatites prepared using wet chemical precipitation. *Materials*, 8(5), 2297–2310. Doi: https://doi.org/10.3390/ma8052297.

[13] Yang Y., Wu Q., Wang M., Long J. & Mao Z. (2014). Hydrothermal synthesis of hydroxyapatite with different morphologies: Influence of supersaturation of the reaction system. *Crystal Growth and Design*, 14(9), 4864–4871. Doi: https://doi.org/10.1021/cg501063j.

[14] Kumar G.S., Sathish L., Raji G. & Girijab E.K. (2015). Utilization of snail shells to synthesize hydroxyapatite nanorods for orthopedic applications. *RSC Advances*, 5(49), 39544–39548. Doi: https://doi.org/10.1039/C5RA04402B.

[15] Rana M., Akhtar N., Rahman S., Jamil H. & Asaduzzaman S.M. (2017). Extraction of hydroxyapatite from bovine and human cortical bone by thermal decomposition and effect of gamma radiation: A comparative study. *International Journal of Complementary & Alternative Medicine*, 8(3), 00263. Doi: https://doi.org/10.15406/ijcam.2017.08.00263.

[16] Akram M., Ahmed R., Shakir I., Ibrahim W.A.W. & Rafaqat H. (2014). Extracting hydroxyapatite and its precursors from natural resources. *Journal of Materials Science*, 49(4), 1461–1475. Doi: https://doi.org/10.1007%2Fs10853-013-7864-x.

[17] Murugan R. & Ramakrishna S. (2005). Porous bovine hydroxyapatite for drug delivery. *Journal of Applied Biomaterials & Biomechanics*, 3(2), 93–97.

[18] Ramesh S., Looa Z.Z., Tana C.Y., Chewb W.J.K., Chinga Y.C., Tarlochanc F., Chandrand H., Krishnasamye S., Bangf L.T. & Sarhan A.A.D. (2018). Characterization of biogenic hydroxyapatite derived from animal bones for biomedical applications. *Ceramics International*, 44(9), 10525–10530. Doi: https://doi.org/10.1016/j.ceramint.2018.03.072.

[19] Ojo O.E., Sekunowo I.O., Ilomuanya M.O., Gbenebor P.O. & Adeosun S.O. (2021). Compositions and thermo-chemical analysis of bovine and caprine bones. *Kufa Journal of Engineering*, 12(3), 56–68. Doi: https://doi.org/10.30572/018/kje/120305.

[20] Ofudje E.A., Rajendran A., Adeogun A.I., Idowu M.A., Kareem S.O. & Pattanayak D.K. (2017). Synthesis of organic derived hydroxyapatite scaffold from pig bone waste for tissue engineering applications. *Advanced Powder Technology*, 29(1), 1–8. Doi: https://doi.org/10.1016/j.apt.2017.09.008.

[21] Venkatesan J. & Kim S.K. (2010). Effect of temperature on isolation and characterization of hydroxyapatite from tuna *(Thunnus obesus)* bone. *Materials*, 3(10), 4761–4772. Doi: https://doi.org/10.3390/ma3104761.

[22] Figueiredo M., Fernando A., Martins G., Freitas J., Judas F. & Figueiredo H. (2010). Effect of the calcination temperature on the composition and microstructure of hydroxyapatite derived from human and animal bone. *Ceramics International*, 36(8), 2383–2393. Doi: https://doi.org/10.1016/j.ceramint.2010.07.016.

[23] Ooi C.Y., Hamdi M. & Ramesh S. (2007). Properties of hydroxyapatite produced by annealing of bovine bone. *Ceramics International*, 33(7), 1171–1177. Doi: https://doi.org/10.1016/j.ceramint.2006.04.001.

[24] Sofronia A.M., Baies R., Anghel E.M., Marinescu C.A. & Tanasescu S. (2014). Thermal and structural characterization of synthetic and natural nanocrystalline hydroxyapatite. *Materials Science and Engineering: C*, 43, 153–163. Doi: https://doi.org/10.1016/j.msec.2014.07.023.

[25] Nga N.K., Giang L.T., Huy T.Q., Viet P.H. & Migliaresi C. (2014). Surfactant-assisted size control of hydroxyapatite nanorods for bone tissue engineering. *Colloids and Surfaces B: Biointerfaces*, 116, 666–673. Doi: https://doi.org/10.1016/j.colsurfb.2013.11.001.

[26] Shavandi A., Bekhit A.E., Ali A. & Sun Z. (2015). Synthesis of nano-hydroxyapatite (nHA) from waste mussel shells using a rapid microwave method. *Materials Chemistry and Physics*, 149–150, 607–616. Doi: https://doi.org/10.1016/j.matchemphys.2014.11.016.

[27] Bahrololoom M.E., Javidi M., Javadpour S. & Ma J. (2009). Characterisation of natural hydroxyapatite extracted from bovine cortical bone ash. *Journal of Ceramic Processing Research*, 10(2), 129–138. Doi: https://doi.org/10.36410/jcpr.2009.10.2.129.

[28] Blanco A., Monte M.C., Campano C., Balea A., Merayo N. & Negro C. (2018). Nanocellulose for industrial use: cellulose nanofibers (CNF), cellulose nanocrystals (CNC), and bacterial cellulose (BC). In: C.M. Hussain, Handbook of Nanomaterials for Industrial Applications *Elsevier,* 74–126. Doi: https://doi.org/10.1016/B978-0-12-813351-4.00005-5.

[29] Zhang H., Yan D., Gedara S.M.K., Marakkalage S.S.F.D., Methlal J.G.K, Han Y.Ch. & Dai H.L. (2017). View effects of crystallinity and surface modification of calcium phosphate nanoparticles on the loading and release of tetracycline hydro-chloride. *IOP Conference Series: Materials Science and Engineering*, 182, 012052. Doi: https://doi.org/10.1088/1757-899X/182/1/012052.

[30] Sanosh K.P., Chu M.-C., Balakrishnan A., Kim T.N. & Cho S.-J. (2009). Preparation and characterization of nano-hydroxyapatite powder using sol-gel technique. *Bulletin of Materials Science*, 32(5), 465–470.

[31] Liu Q., Huang S., Matinlinna J.P., Chen Z. & Pan H. (2013). Insight into biological apatite: physiochemical properties and preparation approaches. *BioMed Research International*. Doi: https://doi.org/10.1155/2013/929748.

[32] Nisar J., Razaq R., Farooq M., Iqbal M., Khan R.A., Sayed M., Shah A. & Rahman I. (2017). Enhanced biodiesel production from *Jatropha* oil using calcined waste animal bones as catalyst. *Renewable Energy,* 101, 111–119. Doi: https://doi.org/10.1016/j.renene.2016.08.048.

[33] Sasikumar S. (2013.) Effect of particle size of calcium phosphate based bioceramic drug delivery carrier on the release kinetics of ciprooxacin hydrochloride: An *in- vitro* study. *Frontiers of Materials Science in China*, 7(3), 261–268. Doi: https://doi.org/10.1007/s11706-013-0216-6.

[34] Netz D.J.A., Sepulveda P., Pandolfelli V.C., Spadaro A.C.C., Alencastre J.B., Lopes Badra Bentley M.V. & Marchetti J.M. (2001). Potential use of gelcasting hydroxyapatite porous ceramic as an implantable drug delivery system. *International Journal of Pharmaceutics*,, 213(1–2), 117–125. Doi: https://doi.org/10.1016/S0378-5173(00)00659-1.

[35] Mohammad N.F., Othman R. & Yeoh F.-Y. (2014). Nanoporous hydroxyapatite preparation methods for drug delivery applications. *Reviews on Advanced Materials Science*, 38, 138–147.